Electron-phonon coupling in transition metals beyond Wang's approximation

Fedor Akhmetov [1,2,*] Igor Milov [3,4] Igor A. Makhotkin,[1] Marcelo Ackermann [1] and Jan Vorberger [2]

[1]*Industrial Focus Group XUV Optics, MESA+ Institute for Nanotechnology, University of Twente, Drienerlolaan 5, 7522NB Enschede, The Netherlands*

[2]*Institute of Radiation Physics, Helmholtz-Zentrum Dresden-Rossendorf (HZDR), Bautzner Landstraße 400, 01328 Dresden, Germany*

[3]*Advanced Research Center for Nanolithography (ARCNL), Science Park 106, 1098 XG Amsterdam, The Netherlands*

[4]*Center for Free-Electron Laser Science CFEL, Deutsches Elektronen-Synchrotron DESY, Notkestr. 85, 22607 Hamburg, Germany*

The electron-phonon coupling is the primary mechanism responsible for material relaxation after ultrafast laser irradiation. However, it remains an elusive variable that is extremely challenging to extract experimentally, especially at high electron temperatures. Various previous theoretical approaches to determine electron-phonon coupling demonstrated large degree of inconsistency. In this paper, we present a first-principles framework for simulating the electron-phonon coupling parameter based on the electron-phonon spectral function, going beyond the approximation introduced by Wang *et al.* [Phys. Rev. B **50**, 8016 (1994)]. Our simulations provide electron-temperature-dependent electron-phonon coupling values for transition metals Ru, Pd, and Au. Our findings reveal significant differences between the values obtained from the exact and approximated spectral functions, thus highlighting the limitations of Wang's approximation at elevated electron temperatures.

I. INTRODUCTION

Ultrafast laser irradiation has become a standard technique in numerous fields, encompassing various spectroscopy techniques [1,2], laser structuring [3,4], medical treatment [5,6], and more. Despite the routine utilization of ultrafast high-power lasers in fundamental research and industrial applications, the underlying physics of ultrafast light-matter interaction is yet to be fully revealed.

When metal absorbs laser irradiation on a femtosecond time scale, electrons transition to high-energy unoccupied states and subsequently undergo transient relaxation toward a thermal distribution. This gives rise to a highly nonequilibrium situation, where the electron temperature significantly exceeds that of the lattice. That occurs within time scales shorter than the electron-lattice relaxation time, typically ranging from 1 to 10 ps, depending on the material under consideration. The process of electron-lattice relaxation is driven by the electron-phonon interaction [7,8].

The simplest yet highly successful model used to describe the evolution of a coupled electron-lattice system under out-of-equilibrium conditions is the famous two-temperature model (TTM). This model was developed by Kaganov *et al.* [9] and later adopted by Anisimov *et al.* [10] for the problems of the ultrafast light-matter interaction. Despite the universally accepted success of TTM in qualitatively describing temperature dynamics in highly excited materials, it may lack quantitative strength, even in the simplest case of ultrafast-heated aluminum [11]. To address the weaknesses of TTM, several different extensions of TTM have been

proposed. These include the so-called nonthermal lattice model (NLM) [11], which accounts for the independent coupling of electrons to different phonon modes; nTTM (density + TTM) [12], allowing the tracing of charge carrier generation in semiconductors; and two-temperature molecular dynamics (TTM-MD) [13,14], which enables the description of possible material transformations on the atomistic level.

At the level of TTM and its successors, the electron-phonon interaction is introduced through the electron-phonon coupling parameter, which establishes the connection between energy exchange and the temperatures of the electrons and lattice. This parameter remains to a large extent unknown, which complicates accurate prediction of the dynamics of ultrafast light-matter interaction. Unfortunately, there is no direct method to measure the electron-phonon coupling at elevated electron and phonon temperatures. State-of-the-art experiments, such as transient optical reflectance measurements [15–18] and ultrafast diffraction techniques [11,19–21], provide information about either integrated electron or lattice response. However, extracting electron-phonon coupling values from these experiments always involves a certain level of approximation.

From a theoretical perspective, there are several models available to determine the electron-phonon coupling parameter. These models include the nonadiabatic tight-binding approach [22], semianalytical methods [23], and *ab initio* approaches [24–26] based on the electron-phonon spectral function (Eliashberg function). Among these, the *ab initio* approach has gained significant attention. However, it is important to note that all of these methods often yield noticeably different values for the electron-phonon coupling parameter. For instance, Ref. [24] reports electron-phonon coupling values in aluminum and gold that are approximately one order

*Corresponding author: f.akhmetov@utwente.nl

of magnitude larger than those derived from the nonadiabatic tight-binding model [22]. Furthermore, no clear evidence exists in favor of one model over the others.

Authors of many studies investigating the electron-phonon coupling at a density functional theory (DFT) level [11,24] employ an approximation for the Eliashberg function that was introduced by Wang *et al.* [27]. It neglects the dependence of the Eliashberg function on the electronic eigenstates. However, this approximation is rather artificial and is valid primarily at relatively low electron temperatures, potentially leading to an overestimation of the electron-phonon coupling at higher levels of electron excitation. Despite the convenience of the exact formalism and its unified formulation for the interaction of ultrafast laser pulses with metals and materials with a band gap, only a few attempts [25,26,28] have been made to go beyond such an approximation.

In this paper, we follow the formalism of Smirnov [26] and calculate the *ab initio* electron-phonon coupling without relying on the assumptions introduced in Wang's approximation. Unlike Smirnov [26], we do not study thermodynamic properties imposed by the electron-phonon coupling parameter, but we focus more on the analysis of Eliashberg function. Furthermore, our method does not require any custom modifications of the existing DFT codes as it is already implemented within the ABINIT [29] software.

In the following sections, we present the theoretical framework underlying our calculations and emphasize the limitations of Wang's approximation. Next, we report the electron-phonon coupling values for gold as well as two other *d*-band metals that have received less attention in previous studies: ruthenium and palladium. Through a thorough analysis of the obtained results, we discuss the implications and highlight the reasons why Wang's approximation should be avoided in future research.

II. MODEL

A. Theory of the electron-phonon coupling

A good starting point for investigating the electron-phonon coupling parameter in solids is the expression for the electron-phonon energy transfer rate. This was derived by Allen [30] from the set of Bloch-Boltzmann-Peierls kinetic equations for electron and phonon distributions:

$$\left(\frac{\partial E_e}{\partial t}\right)_{\text{e-ph}} = 4\pi \sum_{k,q,\nu} \left|g_{k,q}^{\nu}\right|^2 \omega_{\nu,q} S(k, q, T_e, T_{\text{ph}})$$
$$\times \delta(\varepsilon_k - \varepsilon_{k+q} + \omega_q). \quad (1)$$

Here, $g_{k,q}^{\nu}$ is the electron-phonon matrix element corresponding to the scattering of a Bloch state with energy ε_k to state ε_{k+q} with the absorption of a phonon with energy ω_q and polarization ν. Also, $S(k, q, T_e, T_{\text{ph}})$ is a thermal factor with the form:

$$S(k, q, T_e, T_{\text{ph}}) = [f(\varepsilon_k, T_e) - f(\varepsilon_{k+q}, T_e)]$$
$$\times [n(\omega_q, T_{\text{ph}}) - n(\omega_q, T_e)],$$

where $f(\varepsilon, T)$ and $n(\omega, T)$ are Fermi and Bose distribution functions, respectively. Hereafter, we use $\hbar = k_B = 1$.

The electron-phonon coupling parameter $G_{\text{e-ph}}$ represents the energy transfer rate within the well-known TTM [10]:

$$\left(\frac{\partial E_e}{\partial t}\right)_{\text{e-ph}} = G_{\text{e-ph}}(T_{\text{ph}} - T_e).$$

Here, $G_{\text{e-ph}}$ can be elegantly rewritten in terms of the electron-phonon spectral function, also known as the Eliashberg function $\alpha^2 F$, introduced in the Migdal-Eliashberg theory of superconductivity. It demonstrates the effectiveness of phonons in scattering from Bloch state $|\mathbf{k}\rangle$ to $|\mathbf{k} + \mathbf{q}\rangle$ [31]:

$$\alpha^2 F(\varepsilon, \varepsilon', \omega) = 2 \sum_{k,q,\nu} \left|g_{k,q}^{\nu}\right|^2 \delta(\omega - \omega_{\nu,q})$$
$$\times \delta(\varepsilon - \varepsilon_k)\delta(\varepsilon - \varepsilon_{k+q}). \quad (2)$$

This expression differs from those commonly found in the literature by a factor of $1/N(\varepsilon_F)$, where $N(\varepsilon_F)$ is the electronic density of states (DOS) at the Fermi level. This allows for the application of the Eliashberg function in Eq. (2) to the problem of electron-phonon coupling in metals, semiconductors, and insulators. By inserting Eq. (2) into Eq. (1), we obtain the electron-phonon coupling parameter in the form:

$$G_{\text{e-ph}} = \frac{2\pi}{(T_{\text{ph}} - T_e)} \int \omega S(\varepsilon, \omega, T_e, T_{\text{ph}})$$
$$\times \alpha^2 F(\varepsilon, \varepsilon + \omega, \omega) d\omega d\varepsilon. \quad (3)$$

This reduces the problem to the calculation of the Eliashberg function. Equation (3) does not imply any assumptions about the character of scattering, such as scattering in the close vicinity of the Fermi level, which is valid for metals at low temperatures. Therefore, Eq. (3) is rather general and can be used for solids within a wide range of electron temperatures. The only assumptions made are the harmonic nature of ionic motion (phonons) and the Born-Oppenheimer approximation [32].

For the sake of simplicity, authors often apply two approximations for the Eliashberg function. Leveraging the significant difference in the characteristic energy scales of phonons $\omega \sim \omega_D \lesssim 100$ meV and of electrons $\varepsilon \sim \varepsilon_F \sim 1 - 10$ eV, one treats ω as a small addition to ε and expands $S(\varepsilon, \omega, T_e, T_{\text{ph}}), \alpha^2 F(\varepsilon, \varepsilon + \omega, \omega)$ up to the first nonvanishing term:

$$\alpha^2 F(\varepsilon, \varepsilon + \omega, \omega) \approx \alpha^2 F(\varepsilon, \varepsilon, \omega),$$
$$f(\varepsilon + \omega, T_e) \approx f(\varepsilon, T_e) + \frac{\partial f}{\partial \varepsilon} \omega,$$
$$S(\varepsilon, \omega, T_e, T_{\text{ph}}) \approx [n(\omega, T_{\text{ph}}) - n(\omega, T_e)]\left(-\frac{\partial f}{\partial \varepsilon}\right)\omega. \quad (4)$$

This approximation is rather general and appears to be valid for a wide range of materials. Following Wang *et al.* [27], a further approximation can be made for the Eliashberg function by considering the electron-phonon matrix element to be constant over Bloch states:

$$\alpha^2 F(\varepsilon, \varepsilon, \omega) \approx \frac{N^2(\varepsilon)}{N^2(\varepsilon_F)} \alpha^2 F(\varepsilon_F, \varepsilon_F, \omega)$$
$$\equiv \frac{N^2(\varepsilon)}{N^2(\varepsilon_F)} \alpha^2 F(\omega). \quad (5)$$

At high temperatures, the Fermi level must be replaced by the chemical potential $\mu(T_e)$, cf. Eq. (6) in Ref. [33]. Since this approximation assumes a nonzero DOS at the Fermi level $N(\varepsilon_F)$, it can only be applied to metals. Furthermore, its validity should be carefully checked for each metal under consideration.

Equations (4) and (5) yield the well-known expression for the electron-phonon coupling [11,33,34], which we will refer as Wang's approximation:

$$G_{\text{e-ph}} = \frac{2\pi}{(T_{\text{ph}} - T_e)}$$
$$\times \int \omega^2 \alpha^2 F(\omega)[n(\omega, T_{\text{ph}}) - n(\omega, T_e)]d\omega$$
$$\times \int \frac{N^2(\varepsilon)}{N^2(\varepsilon_F)}\left(-\frac{\partial f}{\partial \varepsilon}\right)d\varepsilon. \tag{6}$$

Following Allen [30], this approximation can be further simplified if one considers $\omega_D \ll T_e, T_{\text{ph}}$ and expands the Bose distributions inside the integral over ω:

$$G_{\text{e-ph}} = \pi \lambda \langle \omega^2 \rangle \int \frac{N^2(\varepsilon)}{N(\varepsilon_F)}\left(-\frac{\partial f}{\partial \varepsilon}\right)d\varepsilon. \tag{7}$$

Here, $\lambda \langle \omega^2 \rangle = 2 \int \omega \alpha^2 F(\omega)/N(\varepsilon_F)d\omega$ is the second moment of the Eliashberg function [we restored $1/N(\varepsilon_F)$ factor to recover proper energy^2 dimensions], and λ is the (dimensionless) electron-phonon coupling strength from the McMillan formula [35]. This value can be extracted from experiments, and hence, the electron-phonon coupling parameter can be approximately evaluated with only the knowledge of the electron temperature-dependent DOS. We provide the latter expression as it is widely used in the community [24,27,34].

The Eliashberg functions $\alpha^2 F(\varepsilon, \varepsilon', \omega)$ and $\alpha^2 F(\omega)$ can be obtained as the output from *ab initio* simulations for every electron temperature T_e and the corresponding electron and phonon band structures. In this paper, we calculate the electron-phonon couplings in three different d-band metals, namely, Ru, Pd, and Au, using the exact expression in Eq. (3). We then compare them to the approximated formula in Eq. (6) under conditions typical for ultrafast laser experiments: $T_e \approx$ 10–20 kK. Our calculations reveal that Wang's approximation can deviate significantly from the result obtained with Eq. (3) and even lead to nonphysical behavior of $G_{\text{e-ph}}$ under certain conditions, as demonstrated below.

B. Computational details

All *ab initio* calculations were performed using the ABINIT package [29]. The electronic structures of Ru, Pd, and Au were obtained within the PBE parameterization of the generalized gradient approximation for the exchange-correlation functional [36]. We used the scalar-relativistic version of the norm-conserving Vanderbilt pseudopotential [37] taken from the PSEUDODOJO database [38]. The plane-wave cutoff was selected to ensure the convergence of electron and phonon DOS values, using the following criterion: the residual DOS values change by <1% with further increases in the cutoff value. For the simulations, we used an hexagonal close-packed (hcp) unit cell for Ru, and face-centered cubic (fcc) unit cells for Pd and Au. The lattice parameters of Ru and Pd were taken from

TABLE I. Parameters used in *ab initio* simulations.

Material	E_{cut} (Ha)	Lattice parameter (Bohr)
Ru	40	$a = 5.144, c = 8.119$
Pd	40	7.262
Au	80	7.706

the geometry optimization procedure, whereas for Au, we used the experimental value, which provides better agreement of phonon properties with experimental data. The cutoff and lattice parameter values are provided in Table I. We set the k-point grid to $32 \times 32 \times 32$ points for the self-consistent electron density calculation and $64 \times 64 \times 64$ for the non-self-consistent calculation of the electron wave functions and electron-phonon matrix elements. The self-consistency thresholds were chosen based on the squared wave function residual criterion and were 10^{-14} Ha^2 for electron properties and 10^{-16} Ha^2 for phonon properties calculation.

To obtain the electron temperature-dependent DOS and chemical potential required for Eq. (6), we set the Fermi-Dirac smearing for electron populations and ran several simulations for T_e up to 20 kK.

The phonon frequencies and electron-phonon matrix elements were computed within the density functional perturbation theory (DFPT) on an $8 \times 8 \times 8$ q-point grid. The EPH postprocessing tool [39] enabled us to obtain accurate phonon DOS and the Eliashberg function $\alpha^2 F(\omega)$ via Fourier interpolation of phonon dynamical matrices and DFPT potentials on a dense q-point grid of $32 \times 32 \times 32$, followed by tetrahedron integration over the Brillouin zone.

The current EPH implementation has several restrictions for the $\alpha^2 F(\varepsilon, \varepsilon', \omega)$ calculation: (1) it cannot interpolate matrix elements on a dense q-point grid, (2) it allows only for the Gaussian smearing scheme for Brillouin zone summation, and (3) it supports fixed ϵ, ϵ' grids in a rather narrow window around the Fermi level. The combination of (2) and (3) limits the maximal T_e values for which Eq. (3) can be applied because high T_e results in smearing of the Fermi distribution over large energy windows. Stretching the energy window while keeping a fixed number of grid points means that information about some of the Bloch states will be either completely lost (small Gaussian broadening, states are between grid points) or partially yet inaccurately accounted for (large Gaussian broadening, wings of Gaussians are on grid points). To keep the calculation as accurate as possible, we restricted ourselves to a ±12 eV energy window and a broadening value of 0.272 eV. The chosen energy window is more than sufficient to account for all of the contributing states at $T_e \leqslant 20$ kK.

In the following section, we present the first-principles electron and phonon DOS, phonon band structures, Eliashberg functions, and corresponding electron-phonon coupling parameters. We compare them with available experimental data as well as other theoretical estimations.

III. RESULTS

A. Ru

The calculated electron and phonon properties of Ru are presented in Fig. 1. The total electron DOS for different values
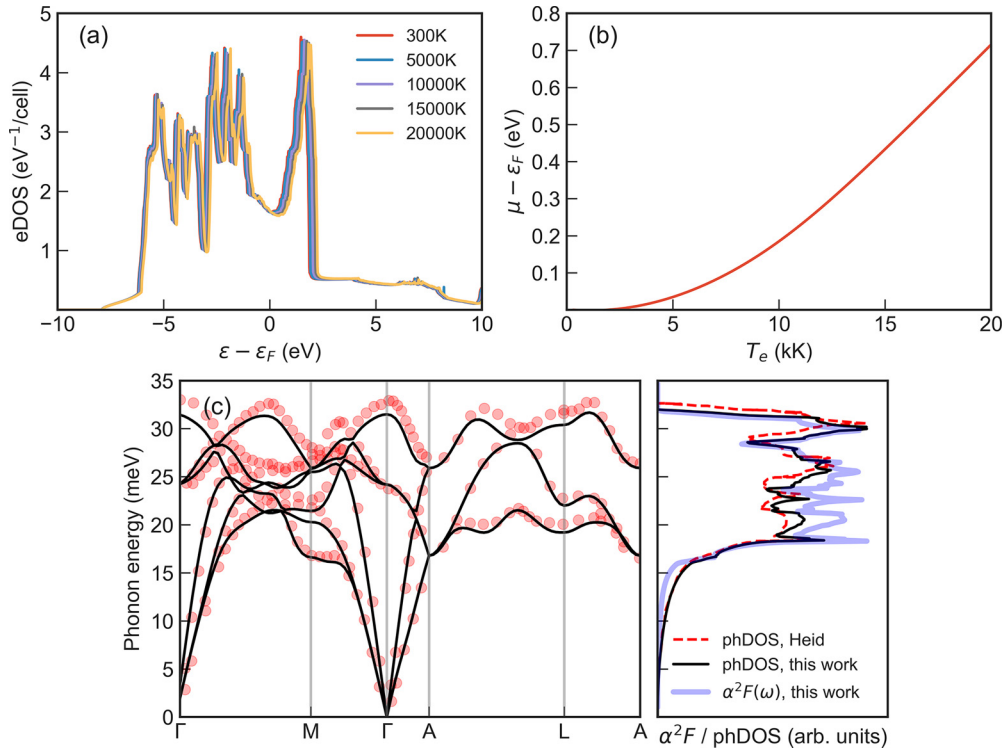
FIG. 1. (a) The electron density of states (DOS) of Ru obtained for different values of T_e. (b) The chemical potential of Ru as a function of T_e. (c) The phonon band structure, phonon DOS, and Eliashberg function $\alpha^2 F(\omega)$ of Ru. The red dots are neutron scattering data, and the red dashed line is the theoretical DOS taken from Ref. [42].

of T_e agrees well with other calculations [40,41]. It features a pronounced pseudogap in the vicinity of the Fermi level. As discussed in more detail below, this pseudogap feature explains the weaker values of $G_{\text{e-ph}}$ at low T_e than those at high T_e, when more energy levels are involved in scattering on phonons. The thermal excitation of electrons from high DOS below the Fermi level to a lower one results in a positive shift of the chemical potential with increasing T_e [Fig. 1(b)].

The calculated phonon band structure and phonon DOS [Fig. 1(c)] are in a very good agreement with the experimental data [42], validating the parameters chosen for the DFPT simulations. The shape of Eliashberg function $\alpha^2 F(\omega)$ is very similar to the shape of the phonon DOS, with slightly higher peaks $< \sim 25$ meV. From the phonon dispersion curve in Fig. 1(c), one can see that this energy range corresponds to acoustic branches. From this, we conclude that electrons tend to couple more strongly to acoustic phonons in Ru.

The full energy-dependent Eliashberg function $\alpha^2 F(\varepsilon, \varepsilon', \omega)$ is presented in Fig. 2. In the case of Ru, it qualitatively resembles a direct product of the electron DOS and $\alpha^2 F(\omega)$, which confirms the assumptions of Wang's approximation. However, contrary to the shape of $N(\varepsilon)$, there is a pronounced asymmetry in the peak intensity below and above the Fermi level. The scattering to or from energy states above the Fermi level contributes considerably less to $G_{\text{e-ph}}$ than expected in Wang's approximation.

Using the calculated Eliashberg functions, we obtained $G_{\text{e-ph}}$ values using Eqs. (3) and (6) and compared them with various theoretical and experimental results (see Fig. 3). At low T_e, Eqs. (3) and (6) yield identical coupling, as expected,

since only the Bloch states very close to the Fermi level scatter on phonons. With increasing T_e, the smearing Fermi distribution involves more and more Bloch states above ε_F in electron-phonon scattering. As we have already pointed out, due to the weaker coupling of those states to phonons compared with Wang's approximation of a constant matrix element [cf. Fig. 1(a) and projections to the ε axis in Fig. 2],
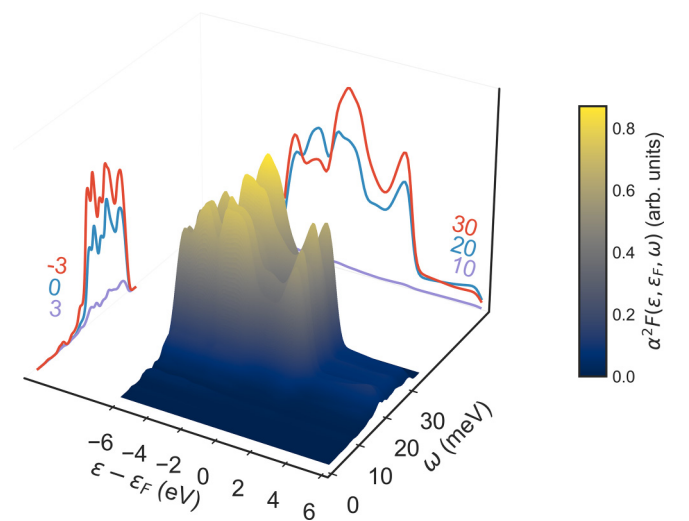

FIG. 2. The electron-energy-resolved Eliashberg function $\alpha^2 F(\varepsilon, \varepsilon_F, \omega)$ of Ru. The contour projections on ω and ϵ axes are drawn for clarity (red, blue, and purple lines), numbers indicate $\varepsilon - \varepsilon_F$ or ω values at which projections were made.
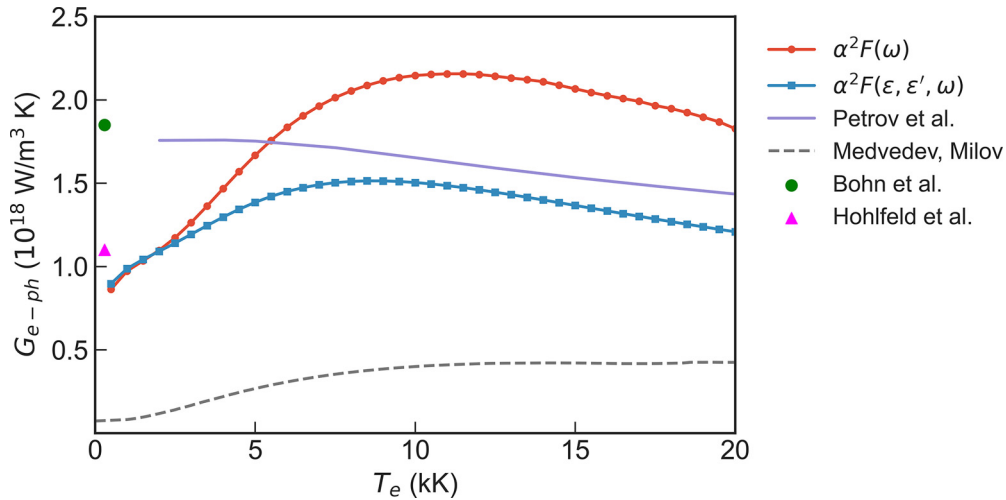
FIG. 3. Electron-phonon coupling parameter $G_{\text{e-ph}}$ in Ru as a function of electron temperature T_e obtained via the exact expression in Eq. (3) (blue) and within the Wang's approximation in Eq. (6) (red). The results are compared with other theoretical data of Petrov *et al.* [41] and Medvedev and Milov [22] as well as experimental estimates by Bohn *et al.* [44] and Hohlfeld *et al.* [15].

the exact expression in Eq. (3) provides noticeably lower $G_{\text{e-ph}}$ values at high T_e.

The low-temperature limit of our $G_{\text{e-ph}}$ values is in qualitative agreement with available experimental data. The work of Petrov *et al.* [41] uses a two-parabolic approximation for the electron DOS as well as Lindhard screening for the electron-ion interaction, assuming free-electron-gas-like behavior. These assumptions seem to be valid at high T_e, providing satisfactory agreement with $G_{\text{e-ph}}$ calculated via the exact expression in Eq. (3). However, the low-temperature values reported in Ref. [41] may be overestimated. Finally, the recently published $G_{\text{e-ph}}$ values calculated within the nonadiabatic tight-binding molecular dynamic (TBMD) formalism [22,43] are an order of magnitude lower. We anticipated such a discrepancy due to (i) the known lack of predictive power of TBMD at low electron temperatures and (ii) the overall divergence between TBMD- and DFT-based approaches for transition metals with half-filled d bands, the origin of which is yet to be analyzed [22].

B. Pd

Figure 4 presents the electron and phonon properties of Pd. The major difference compared with Ru is that the electrons occupy almost the entire d band, and the Fermi level lies on the sharp edge of the d-band DOS. This means that the electrons can be easily thermally excited, leading to a quite significant positive shift of the chemical potential. The phonon band structure and DOS agree less with available neutron scattering data [45] than those of Ru, but they are still sufficiently accurate. The spectral function has a noticeably higher intensity in the range 10–20 meV than the phonon DOS. In this region, DOS and the Eliashberg function are formed by both longitudinal and transverse mode contributions, as follows from Fig. 4(c) (transverse modes in Pd have a small slope around the Γ point). On the contrary, the peaklike region in the range 25–30 meV belongs only to longitudinal modes. This asymmetry of the spectral function may suggest that the electrons in Pd prefer to couple with transverse acoustic phonons rather than longitudinal ones.

The electron energy-dependent spectral function of Pd, shown in Fig. 5, differs quite significantly from the case of Ru, cf. Fig. 2. It no longer resembles a direct product of $N(\varepsilon)$ and $\alpha^2 F(\omega)$, indicating that the underlying assumptions of Wang's approximation are not applicable for Pd. A careful investigation of the (ε, ω) surface reveals that the Bloch states below the Fermi level are primarily coupled to transverse modes ($\omega \lesssim 20$ meV), while the states around the Fermi level tend to couple to longitudinal modes (peak at $\omega \approx 30$ meV).

The comparative analysis of the electron-phonon coupling parameter in Pd calculated via Eqs. (3) and (6) and presented in Fig. 6(a) requires careful attention. First, as it has been pointed out by Smirnov [26], for a Pt metal having very similar band structure, $G_{\text{e-ph}}$ within Wang's approximation decays faster than the exact expression due to the drastic decrease of the contribution of d-band electrons with increasing T_e (cf. fig. 11 in Ref. [26]). Second, many authors [24,34] calculate the coupling via the expression in Eq. (7), placing DOS values at the Fermi level in the denominator in the integral over ε. However, the use of $N(\varepsilon_F)$ at high T_e is somewhat questionable since the electron-phonon scattering involves states around μ. Hence, one should replace $N^2(\varepsilon_F)$ with $N^2(\mu)$ in the denominator of Eq. (6). In many metals with flat DOS in the vicinity of the Fermi level, such a replacement causes only minor changes. In contrast, in Ni, Pd, and Pt, the Fermi level is located on the sharp edge of the d band, and even a minor increase of T_e yields a dramatic increase of inverse DOS $N^{-1}(\mu)$, see Fig. 6(b). As a direct consequence, $G_{\text{e-ph}}$ has a similar increase, which we consider nonphysical [Fig. 6(a), red line]. The exact expression in Eq. (3) is free from ambiguity in the choice of the proper denominator. The calculated coupling parameter behaves smoothly and qualitatively resembles the coupling of Smirnov [26] for Pt.

One may note that the anticipated agreement of our $G_{\text{e-ph}}$ values at low T_e does not hold in Pd. This is due to the use of the Gaussian smearing scheme for $\alpha^2 F(\varepsilon, \varepsilon', \omega)$, which weakens the contribution from scattering around the d-band edge more than it should.
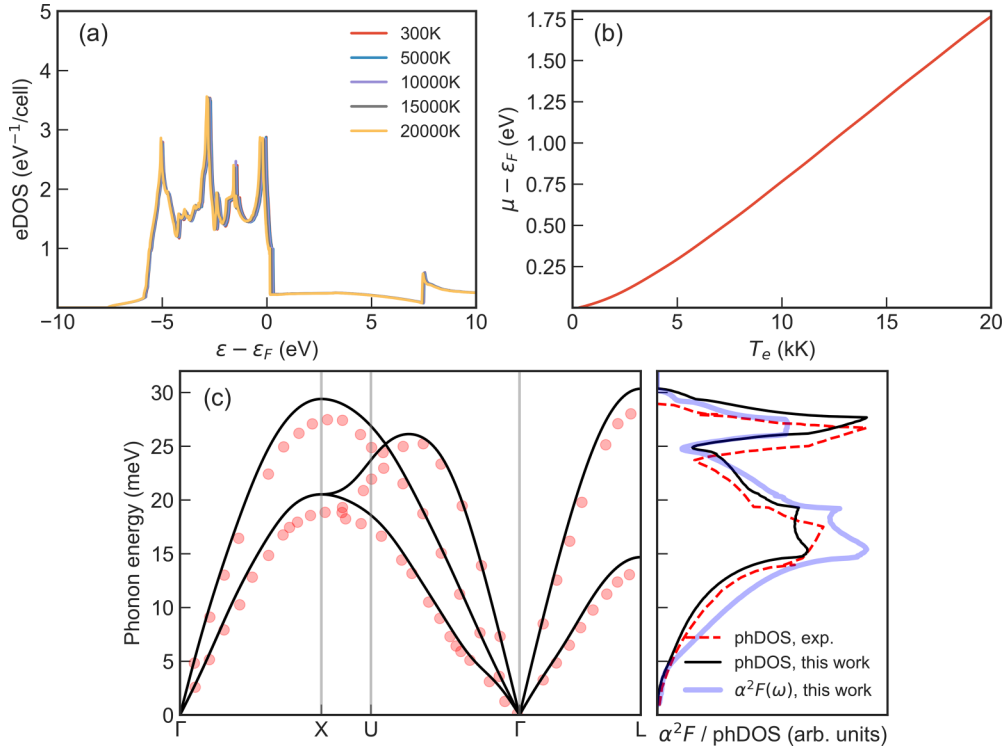
FIG. 4. Same as Fig. 1 but for Pd. The experimental data in (c) are taken from Refs. [45,46].

The G_{e-ph} values calculated with $N^2(\varepsilon_F)$ in Eq. (6) align very well with Ref. [34], as they use the same underlying approximations. At high T_e, when the contribution of d electrons decreases, they overlap with the TBMD-obtained coupling parameter [22,43]. Based on this observation, we could speculate that either TBMD underestimates the contribution of d-band states to the coupling, or DFT overestimates it.

C. Au

The electron and phonon properties of gold used in the calculations of the electron-phonon coupling parameter are
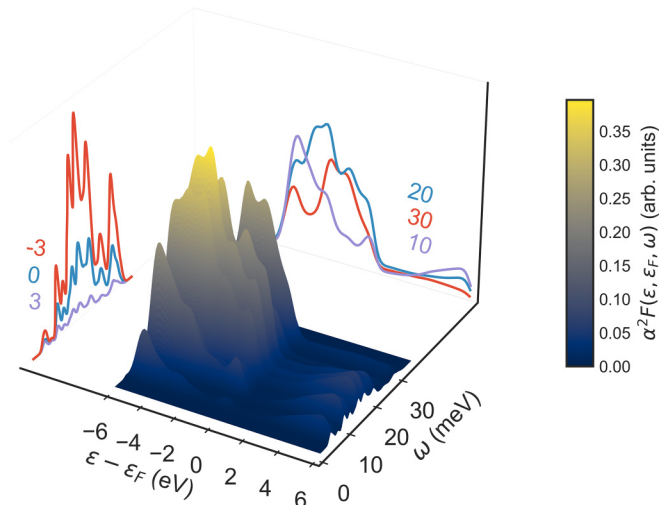

FIG. 5. Same as Fig. 2 but for Pd.

presented in Fig. 7. The behavior of the T_e-dependent electron DOS and chemical potential is typical for noble metals and aligns well with previous reports [24,47]. The obtained phonon band structure agrees well with available neutron scattering data. Like in Pd, another fcc metal, electrons in Au tend to couple more strongly to transverse phonons [cf. Fig. 7(c), black and blue lines].

With the full $\alpha^2 F(\varepsilon, \varepsilon', \omega)$ surface, we can assess the applicability of Wang's approximation in gold. Like in Sec. III A, the spectral function is overall close to the direct product of $N(\varepsilon)$ and $\alpha^2 F(\omega)$. However, electron states below the Fermi level seem to couple less to several phonon modes, smearing out the peaklike shape (see, e.g., region $\omega \approx 5$ meV, -6 eV $\geqslant \varepsilon - \varepsilon_F \leqslant -4$ eV). Therefore, with increasing T_e and smearing of the Fermi distribution, these states start to contribute to G_{e-ph}, and we expect a deviation between the exact coupling parameter and Wang's approximation (see Fig. 8).

Figure 9 displays the electron-phonon coupling parameter in Au compared with numerous other theoretical works as well as several experimental data at low T_e. Although many other low-temperature experimental values for G_{e-ph} exist (cf. Refs. [22,51–55]), they are very close to each other and to the shown points of Hohlfeld [15] and Sokolowski-Tinten [49], and hence, we decided not to depict them explicitly. The G_{e-ph} values obtained within Wang's approximation in Eq. (6) agree satisfactorily with the results of Li *et al.* [34], calculated via Eq. (7). The slight difference may stem from different coupling strengths: $\lambda\langle\omega^2\rangle = 21.5$ meV^2 by Li *et al.* [34] and $\lambda\langle\omega^2\rangle = 19.2$ meV^2 in this paper.

As discussed above, although $\alpha^2 F(\varepsilon, \varepsilon', \omega)$ in Au is close to Wang's approximation, the electron-phonon coupling parameter calculated with the exact expression increases more
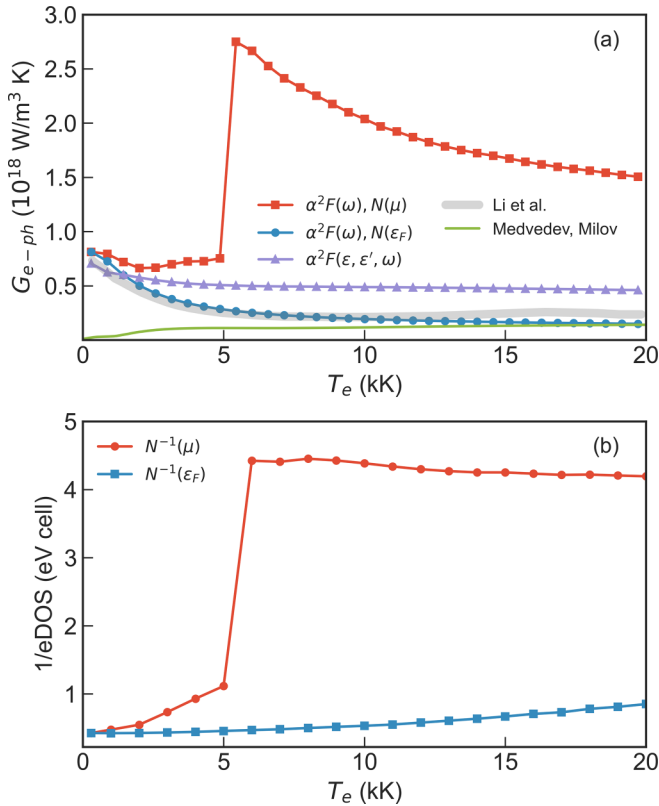
FIG. 6. (a) Electron-phonon coupling parameter $G_{e\text{-ph}}$ in Pd as a function of electron temperature T_e obtained via the exact expression in Eq. (3) (purple) and within Wang's approximation in Eq. (6) with electron density of states (DOS) values taken at the Fermi level $N(\varepsilon_F)$ (blue) and the temperature-dependent chemical potential $N(\mu)$ (red). The results are compared with simulations of Li *et al.* [34] and Medvedev and Milov [22]. (b) The dependence of $N^{-1}(\varepsilon_F)$ (blue) and $N^{-1}(\mu)$ (red) on T_e.

slowly with temperature. The $G_{e\text{-ph}}$ based on $\alpha^2 F(\varepsilon, \varepsilon', \omega)$ largely reproduces the results of Smirnov [26] and Brown *et al.* [25], who also use the exact formula in Eq. (3), which validates our results as well as $\alpha^2 F(\varepsilon, \varepsilon', \omega)$ produced by the EPH postprocessor for the ABINIT package.

The low-T_e $G_{e\text{-ph}}$ data obtained from TBMD simulations [43] are in satisfactory agreement with present simulations in the case of NRL parameterization yet noticeably lower in the case of DFTB parameterization. When T_e increases, a situation directly opposite to Pd is observed: d-band states start to contribute in electron-phonon scattering, resulting in a significant deviation of TBMD data from *ab initio* results. This is an additional confirmation of the speculation made above: the TBMD approach seems to underestimate the contribution of d-band electrons to $G_{e\text{-ph}}$ in respect to DFT. However, we shall make a point that the results of Petrov *et al.* (Petrov *et al.*, 0.6) [23] and Migdal *et al.* [48], both based on two-parabolic approximation and Lindhard dielectric screening, agree with the TBMD data. Let us discuss this agreement in detail.

The electron-phonon matrix elements $g_{k,q}^\nu$ represent matrix elements of the electron-ion potential. Naturally, the most suitable form for this potential is the bare electron-nucleus Coulomb interaction screened by the dielectric function. It

is very difficult to obtain an accurate dielectric function; one usually restricts oneself to lowest order of perturbation theory and uses the dielectric function within the random-phase approximation (RPA). That is exactly how the electron-phonon matrix elements were calculated in Refs. [23,48] since the Lindhard function they have used is the simplest kind of RPA, and it is known to overestimate dielectric screening, resulting in weaker electron-phonon coupling.

In contrast, the electron-phonon matrix elements in DFPT involve derivatives of the self-consistent Kohn-Sham potential with respect to phonon wave vector **q**. As discussed by Giustino [32], the DFPT scheme is equivalent to screening the Coulomb interaction using a RPA + xc level dielectric function, which incorporates local-field corrections originating from exchange and correlation (xc) effects. It is widely accepted that such an RPA + xc dielectric function provides a more accurate approximation.

Surprisingly, a simple rescaling of Petrov's coupling to the experimental electron-phonon coupling constant (Petrov *et al.*, cor) yields the same values as our DFPT-based simulations. This suggests that the rescaling can be interpreted as the renormalization of the dielectric function to incorporate band structure as well as local-field effects. The noble nature of gold (electron-gas-like behavior of conduction band electrons) may be the reason why such a simple rescaling recovers proper RPA + xc based on Bloch states obtained from DFT.

We also highlight the recent experiment by Mo *et al.* [50] on ultrafast electron diffraction measurement of melting in thin gold films. The observed melting dynamics and energy threshold for the transition between heterogeneous and homogeneous melting regimes suggest a T_e-dependent $G_{e\text{-ph}}$, like those reported in Refs. [22,43,48]. However, the measurements of the experiment were fitted using constant $G_{e\text{-ph}}$ values corresponding to different absorbed energy density regimes, which do not fully reflect the dynamics of electron-lattice energy exchange. Therefore, the values of electron-phonon coupling extracted from this experiment should be considered an effective coupling parameter for each absorbed energy density, and not as T_e-dependent $G_{e\text{-ph}}$. A more rigorous two-temperature analysis by Smirnov [26] was able to reproduce the dynamics of homogeneous melting but struggled with partial or heterogeneous melting regimes. Furthermore, a more advanced TTM-MD analysis [56] suggested that the experimentally observed dynamics cannot be reproduced using any reasonable model for the electron-phonon coupling parameter. Therefore, the high-T_e experimental points should be used for validation of theoretical models only with great caution.

IV. CONCLUSIONS

We conducted first-principles simulations of the electron-phonon coupling parameter $G_{e\text{-ph}}$ in transition metals based on Allen's [30] theory of thermal relaxation in the coupled electron-phonon system. We calculated the electron energy-dependent Eliashberg functions entering the exact expression for $G_{e\text{-ph}}$. However, the accuracy of the underlying theory is limited by (i) the formal accuracy of the Boltzmann equation, (ii) the Born-Oppenheimer approximation and the phonon picture, and (iii) certain approximations
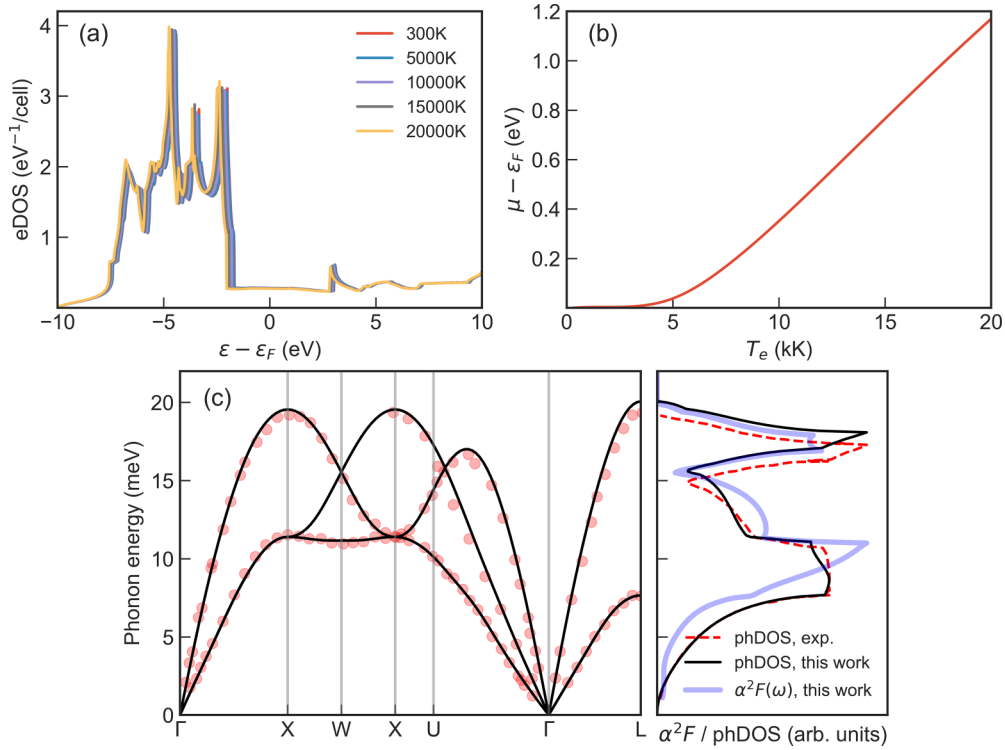
FIG. 7. Same as Fig. 1 but for Au. The experimental data in (c) are taken from Ref. [45].

imposed by the DFT framework, such as the accuracy of the chosen exchange-correlation functional and numerical parameters. We evaluated these Eliashberg functions in the low-temperature limit, as they show minor temperature dependence in the range of $T_e \leqslant 20$ kK considered here. Nonetheless, for higher T_e values, the evaluation of the Eliashberg functions for each temperature is necessary, as follows from Ref. [33].

The obtained Eliashberg functions for d-band metals, specifically Ru, Pd, and Au, were analyzed in detail to determine the materials and conditions under which they can be approximated by Wang's expression in Eq. (5). The values of $G_{\text{e-ph}}$ for Ru, Pd, and Au were compared with experimental data as well as previous theoretical simulations that employed various approximations. These approximations included semianalytical expressions, the nonadiabatic tight-binding molecular dynamics (TBMD) approach, the standard Wang's approximation, and the variations of the exact theory that do not involve any approximations for the Eliashberg function.

Our findings indicate that the DFT-based electron-phonon coupling values are consistently higher than TBMD values. Based on the analysis of the high-T_e behavior of coupling, we attribute this divergence to the underestimation of the contribution of d-band states to the electron-phonon coupling in TBMD. We also showed that Wang's approximation does not accurately account for the coupling between different electron states and different phonon modes, resulting in larger $G_{\text{e-ph}}$ values in the case of Ru and Au and weaker in the case of Pd.

The agreement of our results obtained for Au with previous works [25,26] validates the method of the Eliashberg function calculation provided by the EPH tool (part of the ABINIT simulation package [29]). This means that specialists in material science and condensed matter physics have a ready-to-use tool for accurate simulations of the electron-phonon coupling parameter, which is seamlessly applicable for metals, semiconductors, and dielectrics.
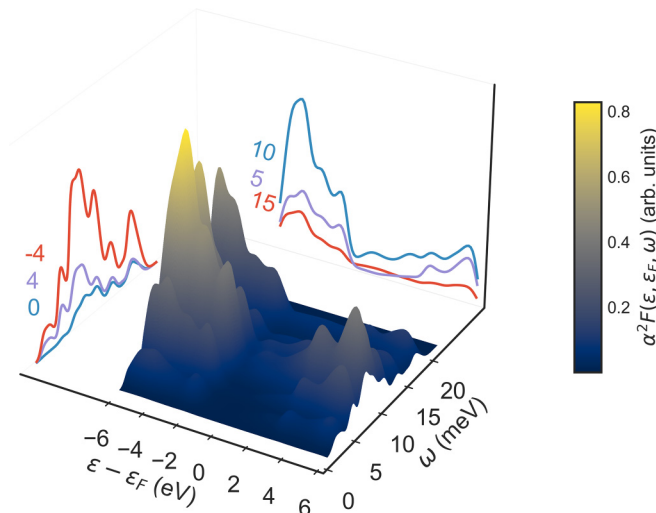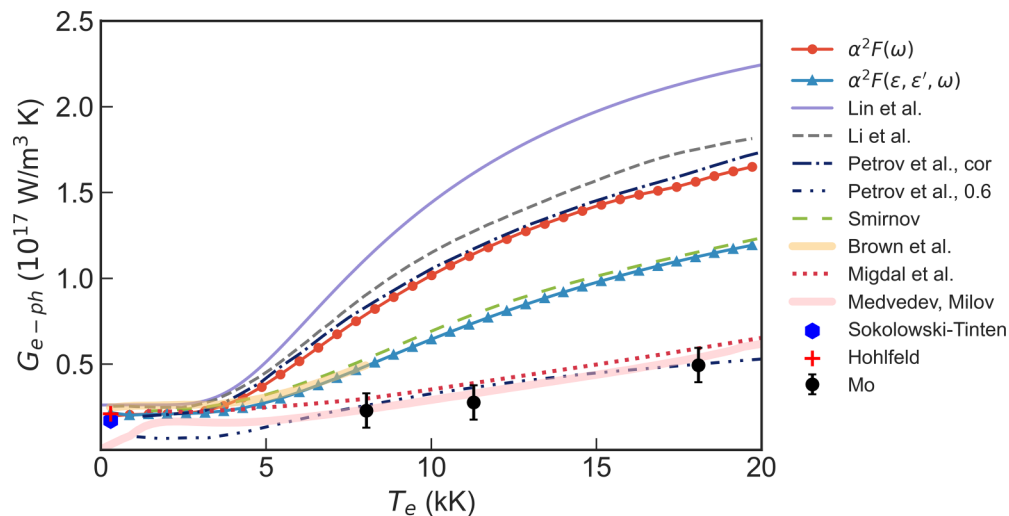
FIG. 8. Same as Fig. 2 but for Au.

FIG. 9. Electron-phonon coupling parameter $G_{\text{e-ph}}$ in Au as a function of electron temperature T_e obtained via the exact expression in Eq. (3) (blue) and within Wang's approximation in Eq. (6) (red). Theoretical results to compare with are taken from Lin *et al.* [24], Li *et al.* [34], Petrov *et al.* [23] (both cor and 0.6, see fig. 6 there), Smirnov [26], Brown *et al.* [25], Migdal *et al.* [48], and Medvedev and Milov [22]; experimental points are from Sokolowski-Tinten *et al.* [49], Hohlfeld *et al.* [15], and Mo *et al.* [50].

[1] M. Maiuri, M. Garavelli, and G. Cerullo, Ultrafast spectroscopy: State of the art and open challenges, J. Am. Chem. Soc. **142**, 3 (2020).

[2] A. Kirilyuk, A. V. Kimel, and T. Rasing, Ultrafast optical manipulation of magnetic order, Rev. Mod. Phys. **82**, 2731 (2010).

[3] A. P. Caricato, A. Luches, and M. Martino, Laser fabrication of nanoparticles, in *Handbook of Nanoparticles* (Springer International Publishing, Cham, 2016), pp. 407–428.

[4] K. Sugioka and Y. Cheng, Ultrafast lasers—Reliable tools for advanced materials processing, Light Sci. Appl. **3**, e149 (2014).

[5] H. Lubatschowski, A. Heisterkamp, F. Will, A. I. Singh, J. Serbin, A. Ostendorf, O. Kermani, R. Heermann, H. Welling, and W. Ertmer, Medical and biological applications for ultrafast laser pulses, Proc. SPIE **4830**, 537 (2003).

[6] C. L. Hoy, O. Ferhanoğlu, M. Yildirim, K. H. Kim, S. S. Karajanagi, K. M. C. Chan, J. B. Kobler, S. M. Zeitels, and A. Ben-Yakar, Clinical ultrafast laser surgery: Recent advances and future directions, IEEE J. Sel. Top. Quantum Electron. **20**, 242 (2014).

[7] B. Rethfeld, K. Sokolowski-Tinten, D. Von Der Linde, and S. I. Anisimov, Timescales in the response of materials to femtosecond laser excitation, Appl. Phys. A **79**, 767 (2004).

[8] B. Rethfeld, D. S. Ivanov, M. E. Garcia, and S. I. Anisimov, Modelling ultrafast laser ablation, J. Phys. D **50**, 193001 (2017).

[9] M. I. Kaganov, I. M. Lifshitz, and L. V. Tanatarov, Relaxation between electrons and the crystalline lattice, Zh. Eksp. Teor. Fiz. **31**, 232 (1957) [Sov. Phys. JETP **4**, 173 (1957)].

[10] S. Anisimov, B. Kapeliovich, and T. Perel'man, Electron emission from metal surfaces exposed to ultrashort laser pulses, Zh. Eksp. Teor. Fiz. **66**, 776 (1974) [Sov. Phys. JETP **39**, 375 (1974)].

[11] L. Waldecker, R. Bertoni, R. Ernstorfer, and J. Vorberger, Electron-phonon coupling and energy flow in a simple metal beyond the two-temperature approximation, Phys. Rev. X **6**, 021003 (2016).

[12] H. M. van Driel, Kinetics of high-density plasmas generated in Si by 1.06- and 0.53- μm picosecond laser pulses, Phys. Rev. B **35**, 8166 (1987).

[13] D. Ivanov and L. Zhigilei, Combined atomistic-continuum modeling of short-pulse laser melting and disintegration of metal films, Phys. Rev. B **68**, 064114 (2003).

[14] D. M. Duffy and A. M. Rutherford, Including the effects of electronic stopping and electron-ion interactions in radiation damage simulations, J. Phys.: Condens. Matter **19**, 016207 (2007).

[15] J. Hohlfeld, S.-S. Wellershoff, J. Güdde, U. Conrad, V. Jähnke, and E. Matthias, Electron and lattice dynamics following optical excitation of metals, Chem. Phys. **251**, 237 (2000).

[16] P. M. Norris, A. P. Caffrey, R. J. Stevens, J. M. Klopf, J. T. McLeskey, and A. N. Smith, Femtosecond pump-probe nondestructive examination of materials (invited), Rev. Sci. Instrum. **74**, 400 (2003).

[17] P. E. Hopkins and P. M. Norris, Substrate influence in electron-phonon coupling measurements in thin Au films, Appl. Surf. Sci. **253**, 6289 (2007).

[18] J. L. Hostetler, A. N. Smith, D. M. Czajkowsky, and P. M. Norris, Measurement of the electron-phonon coupling factor

dependence on film thickness and grain size in Au, Cr, and Al, Appl. Opt. **38**, 3614 (1999).

[19] G. Sciaini and R. J. Miller, Femtosecond electron diffraction: Heralding the era of atomically resolved dynamics, Rep. Prog. Phys. **74**, 096101 (2011).

[20] P. M. Kraus, M. Zürch, S. K. Cushing, D. M. Neumark, and S. R. Leone, The ultrafast x-ray spectroscopic revolution in chemical dynamics, Nat. Rev. Chem. **2**, 82 (2018).

[21] M. Mo, Z. Chen, and S. Glenzer, Ultrafast visualization of phase transitions in nonequilibrium warm dense matter, MRS Bull. **46**, 694 (2021).

[22] N. Medvedev and I. Milov, Electron-phonon coupling in metals at high electronic temperatures, Phys. Rev. B **102**, 064302 (2020).

[23] V. Y. Petrov, N. A. Inogamov, and K. P. Migdal, Thermal conductivity and the electron-ion heat transfer coefficient in condensed media with a strongly excited electron subsystem, JETP Lett. **97**, 20 (2013).

[24] Z. Lin, L. V. Zhigilei, and V. Celli, Electron-phonon coupling and electron heat capacity of metals under conditions of strong electron-phonon nonequilibrium, Phys. Rev. B **77**, 075133 (2008).

[25] A. M. Brown, R. Sundararaman, P. Narang, W. A. Goddard, and H. A. Atwater, *Ab initio* phonon coupling and optical response of hot electrons in plasmonic metals, Phys. Rev. B **94**, 075120 (2016).

[26] N. A. Smirnov, Copper, gold, and platinum under femtosecond irradiation: Results of first-principles calculations, Phys. Rev. B **101**, 094103 (2020).

[27] X. Y. Wang, D. M. Riffe, Y.-S. Lee, and M. C. Downer, Time-resolved electron-temperature measurement in a highly excited gold target using femtosecond thermionic emission, Phys. Rev. B **50**, 8016 (1994).

[28] B. Arnaud and Y. Giret, Electron cooling and Debye-Waller effect in photoexcited bismuth, Phys. Rev. Lett. **110**, 016405 (2013).

[29] X. Gonze, B. Amadon, G. Antonius, F. Arnardi, L. Baguet, J. M. Beuken, J. Bieder, F. Bottin, J. Bouchet, E. Bousquet *et al.*, The ABINIT project: Impact, environment and recent developments, Comput. Phys. Commun. **248**, 107042 (2020).

[30] P. B. Allen, Theory of thermal relaxation of electrons in metals, Phys. Rev. Lett. **59**, 1460 (1987).

[31] P. B. Allen and B. Mitrović, Theory of superconducting T_c, Solid State Phys. **37**, 1 (1983).

[32] F. Giustino, Electron-phonon interactions from first principles, Rev. Mod. Phys. **89**, 015003 (2017).

[33] J. Zhang, R. Qin, W. Zhu, and J. Vorberger, Energy relaxation and electron-phonon coupling in laser-excited metals, Materials **15**, 1902 (2022).

[34] Y. Li and P. Ji, *Ab initio* calculation of electron temperature dependent electron heat capacity and electron-phonon coupling factor of noble metals, Comput. Mater. Sci. **202**, 110959 (2022).

[35] W. L. McMillan, Transition temperature of strong-coupled superconductors, Phys. Rev. **167**, 331 (1968).

[36] J. P. Perdew, K. Burke, and M. Ernzerhof, Generalized gradient approximation made simple, Phys. Rev. Lett. **77**, 3865 (1996).

[37] D. R. Hamann, Optimized norm-conserving Vanderbilt pseudopotentials, Phys. Rev. B **88**, 085117 (2013).

[38] M. J. van Setten, M. Giantomassi, E. Bousquet, M. J. Verstraete, D. R. Hamann, X. Gonze, and G. M. Rignanese, The PSEUDODOJO: Training and grading a 85 element optimized norm-conserving pseudopotential table, Comput. Phys. Commun. **226**, 39 (2018).

[39] G. Brunin, H. P. C. Miranda, M. Giantomassi, M. Royo, M. Stengel, M. J. Verstraete, X. Gonze, G. M. Rignanese, and G. Hautier, Phonon-limited electron mobility in Si, GaAs, and GaP with exact treatment of dynamical quadrupoles, Phys. Rev. B **102**, 094308 (2020).

[40] A. V. Lugovskoy, M. P. Belov, O. M. Krasilnikov, and Y. K. Vekilov, Stability of the hcp ruthenium at high pressures from first principles, J. Appl. Phys. **116**, 103507 (2014).

[41] Y. Petrov, K. Migdal, N. Inogamov, V. Khokhlov, D. Ilnitsky, I. Milov, N. Medvedev, V. Lipp, and V. Zhakhovsky, Ruthenium under ultrafast laser excitation: Model and dataset for equation of state, conductivity, and electron-ion coupling, Data Brief **28**, 104980 (2020).

[42] R. Heid and L. Pintschovius, W. Reichardt, and K. P. Bohnen, Anomalous lattice dynamics of ruthenium, Phys. Rev. B **61**, 12059 (2000).

[43] F. Akhmetov, N. Medvedev, I. Makhotkin, M. Ackermann, and I. Milov, Effect of atomic-temperature dependence of the electron-phonon coupling in two-temperature model, Materials **15**, 5193 (2022).

[44] M. Bonn, D. N. Denzler, S. Funk, M. Wolf, S.-S. Wellershoff, and J. Hohlfeld, Ultrafast electron dynamics at metal surfaces: Competition between electron-phonon coupling and hot-electron transport, Phys. Rev. B **61**, 1101 (2000).

[45] P. H. Dederichs, H. Schober, and D. J. Sellmyer, *Phonon States of Elements. Electron States and Fermi Surfaces of Alloys* (Springer, Berlin, 1981).

[46] S. S. Setayandeh, C. J. Webb, and E. M. Gray, Progress in solid state chemistry electron and phonon band structures of palladium and palladium hydride: A review, Prog. Solid State Chem. **60**, 100285 (2020).

[47] E. Bévillon, J. P. Colombier, V. Recoules, and R. Stoian, Free-electron properties of metals under ultrafast laser-induced electron-phonon nonequilibrium: A first-principles study, Phys. Rev. B **89**, 115117 (2014).

[48] K. P. Migdal, D. K. Il'Nitsky, Y. V. Petrov, and N. A. Inogamov, Equations of state, energy transport and two-temperature hydrodynamic simulations for femtosecond laser irradiated copper and gold, J. Phys.: Conf. Ser. **653**, 012086 (2015).

[49] K. Sokolowski-Tinten, X. Shen, Q. Zheng, T. Chase, R. Coffee, M. Jerman, R. K. Li, M. Ligges, I. Makasyuk, M. Mo *et al.*, Electron-lattice energy relaxation in laser-excited thin-film Au-insulator heterostructures studied by ultrafast MeV electron diffraction, Struct. Dyn. **4**, 054501 (2017).

[50] M. Z. Mo, Z. Chen, R. K. Li, M. Dunning, B. B. L. Witte, J. K. Baldwin, L. B. Fletcher, J. B. Kim, A. Ng, R. Redmer *et al.*, Heterogeneous to homogeneous melting transition visualized with ultrafast electron diffraction, Science **360**, 1451 (2018).

[51] S. D. Brorson, A. Kazeroonian, J. S. Moodera, D. W. Face, T. K. Cheng, E. P. Ippen, M. S. Dresselhaus, and G. Dresselhaus, Femtosecond room-temperature measurement of the electron-phonon coupling constant in metallic superconductors, Phys. Rev. Lett. **64**, 2172 (1990).

[52] L. Guo and X. Xu, Ultrafast spectroscopy of electron-phonon coupling in gold, J. Heat Transfer **136**, 122401 (2014).

[53] T. G. White, P. Mabey, D. O. Gericke, N. J. Hartley, H. W. Doyle, D. McGonegle, D. S. Rackstraw, A. Higginbotham, and G. Gregori, Electron-phonon equilibration in laser-heated gold films, Phys. Rev. B **90**, 014305 (2014).

[54] A. Nakamura, T. Shimojima, M. Nakano, Y. Iwasa, and K. Ishizaka, Electron and lattice dynamics of transition metal thin films observed by ultrafast electron diffraction and transient optical measurements, Struct. Dyn. **3**, 064501 (2016).

[55] Q. Zheng, X. Shen, K. Sokolowski-Tinten, R. K. Li, Z. Chen, M. Z. Mo, Z. L. Wang, S. P. Weathersby, J. Yang, M. W. Chen *et al.*, Dynamics of electron-phonon coupling in bicontinuous nanoporous gold, J. Phys. Chem. C **122**, 16368 (2018).

[56] M. I. Arefev, M. V. Shugaev, and L. V. Zhigilei, Kinetics of laser-induced melting of thin gold film: How slow can it get? Sci. Adv. **8**, eabo2621 (2022).

[57] www.surf.nl.